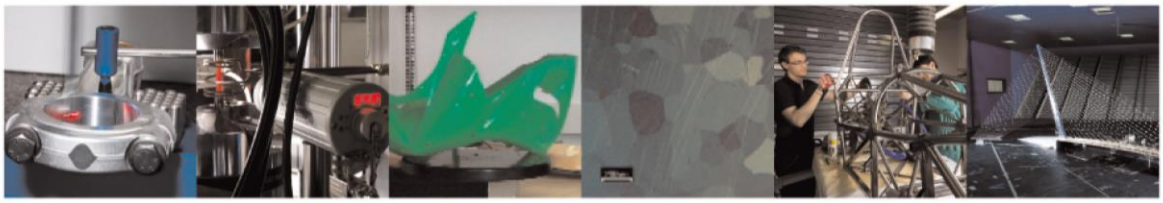

Evaluation of Self-Mixing Interferometry Performance in the Measurement of Ablation Depth

Demir, Ali Gokhan; Colombo, Paolo; Norgia, Michele; Previtali, Barbara

This is a post-peer-review, pre-copyedit version of an article published in IEEE TRANSACTIONS ON INSTRUMENTATION AND MEASUREMENT. The final authenticated version is available online at: http://dx.doi.org/10.1109/TIM.2016.2596038

Evaluation of self-mixing interferometry performance in the measurement of ablation depth

Ali Gökhan Demir[1]*, Paolo Colombo[1], Michele Norgia[2], Barbara Previtali[1]

[1]Department of Mechanical Engineering, Politecnico di Milano, Via La Masa 1, 20156 Milan, Italy

[2]Department of Electronics, Information and Bioengineering, Politecnico di Milano, Via Ponzio 34/5, 20133 Milan, Italy

*Corresponding author: aligokhan.demir@polimi.it; Tel: +39 02 2399 8590; Fax: +39 02 2399 8585

Evaluation of self-mixing interferometry performance in the measurement of ablation depth

Abstract

This paper studies self-mixing interferometry for measuring ablation depth during laser percussion drilling of TiAlN ceramic coating. The measurement performance of self-mixing interferometry was investigated in a large processing range producing blind microholes with depths below and beyond the average coating thickness. Signal characteristics of the measurement system was evaluated indicating sources of disturbance. The self-mixing interferometry measurements were compared to a conventional measurement device based on focus variation microscopy to evaluate the measurement error. The measurement error classes were defined, as well as defining the related error sources. The results depict that the measurement error was independent from the processing condition, hence the hole geometry and ablation rate. For 76% of cases measurement error was below the intrinsic device resolution obtainable by simple fringe counting of half a wavelength ($\lambda/2$=0.393 μm).

Keywords: Laser microdrilling, self-mixing interferomety, laser surface texturing, laser ablation

1. Introduction

Laser ablation is a flexible micromachining process that enables high precision non-contact machining. Due the non-contact nature of the process, the control of machining depth is difficult. In particular, the control of machining depth on surface coatings for laser surface texturing applications becomes of paramount importance. In the case of thin ceramic surface coatings on steel substrates, high accuracy in the machining depth is required to avoid damage on coating by substrate contamination [1]. The applied coating layer is characterized by limited thickness, in the order of 2-15 μm. When the machining depth exceeds the coating thickness, the ablation conditions change drastically since the steel substrate behaves differently during the interaction with the laser beam [2]. Particularly in percussion drilling, molten steel from the substrate is deposited at the entrance of the blind hole. For laser surface texturing in view of friction applications, where a great number of microholes is realized over large areas to make a reservoir of solid or liquid lubricant [3], substrate reach can cause coating failure [2]. Thus, online monitoring capabilities are required to overcome process variations during the machining of large area components.

Several techniques for ablation depth monitoring have been proposed in literature. Methods exploiting acoustic emission of the process [4] and mechanical vibration due to wavefront expansion [5] have been proposed. However, the majority of the techniques employ optical methods. Depending on the used method direct or indirect measurement of the ablation depth can be made. Concerning the indirect methods, use of photodiodes (PDs) [6],[7] and optical emission spectrum [8]-[12] are the methods, which allow to correlate

the signal to the measured depth. In the case of optical emission spectrum the signal can also be employed to detect change of material layer by observing the presence of a new signal component, such as plasma emission lines. Direct measurement methods commonly rely on imaging the hole itself using a probe light and a sensor. Depending on the sensor type, the measurement can be carried out in 3D or only single dimensional, hence the depth. For this purpose, Döring et. al. used a high resolution imaging systems based on CCD camera, for visualization of ablation depth in transparent materials [13]. Interferometric methods have also been implemented to measure the ablation depth, at the end of and during the process. Papazoglou et. al. used white light interferometry implemented into the optical chain of the processing laser, which could acquire high resolution 3D images of the ablation area after the process [14]. Webster et. al. proposed to use Fourier domain optical coherence tomography (OCT) for faster acquisition of ablation depth [15]-[18]. The technique was shown to perform with 6.2 μm depth and 100ns time resolution. On the other hand, self-mixing interferometry (SMI) is another appealing option as a high resolution point displacement measurement technique [19], which can be adapted in laser micromachining to monitor ablation depth [20]-[22]. The depth resolution is intrinsically high, since it is half the wavelength of the interferometer (typically $\lambda/2<0.5\mu m$). The system also flexibly allows for increasing the temporal resolution, as MHz level electronic bandwidths are achievable. Previous work showed that stable SMI measurements in ceramic coatings ablation was possible in presence of a side gas jet [23]. Although its potential use in ablation depth monitoring has been proven, the measurement performance of SMI in microdrilling depth measurement has not been studied previously. SMI has been used and characterized extensively for measurement of displacement [24],[25], distance [26], vibration [27], speed [19] and flow [28],[29] in different dimensional scales. On the other hand, ablation depth monitoring requires demanding measurement accuracy, in a scale comparable to the resolution of the device. Moreover, the ablation phenomenon itself reduces the signal quality in measurement, which adds up to the complexity of the problem. Characterization of the measurement performance is of high importance when the method should monitor depth of blind holes on coatings with limited thickness (1-15 μm). Hence, the number of fringes to appear will be few, typically between 2 and 35. Errors in fringe appearance and counting accordingly can become comparable to the measured quantity.

In this work, SMI is applied in the laser percussion drilling of TiAlN ceramic coating deposited on AISI D2 steel. The 12 μm thick TiAlN coating was drilled with a pulsed green fibre laser, while the SMI was applied with a 785 nm laser diode for micro hole depth measurement. In particular, the ablation depth measurement system is required to avoid incorrect measurement in proximity of coating-substrate interface. Accordingly, the measurement requirements were explained. The signal characteristics were compared to

the signals obtained with conventional measurement systems. The measurement accuracy of the employed method was evaluated by comparison with a conventional surface measurement instrument based on focus-variation microscopy.

2. Ablation depth monitoring system based on self-mixing interferometry

Conventional interferometry technique used for displacement measurement (Michelson interferometry) uses a reference and a measurement arm. Typically, two measurement channels are used, otherwise the displacement direction is ambiguous. SMI exploits interference occurring in the laser cavity due to back-reflected light [19]. Laser diodes (LD) are the most common choice for a self-mixing interferometer. A photodiode (PD) is usually available, mounted at the rear mirror of the laser chip, which is used to measure the power fluctuations due to the interference. As shown in Fig. 1.a, in a SMI configuration, a small portion of the emitted beam is back reflected from a remote target enters the cavity after being attenuated in the external cavity. The reflected laser field phase depends on the distance of the reflecting body at a given time instance [19]. In SMI, the back reflected field E_r, adds to the lasing field E_l, modulating its amplitude and frequency. The interferometric phase can be retrieved from the change of the optical power measured. The periodic function of the interferometric phase, hence the signal shape, depends on the feedback parameter (C). Feedback parameter depends on the laser diode design and characteristics as well as optical attenuation in the external cavity. An increase in the optical attenuation results in the decrease of the feedback parameter, hence change of the signal shape. In very weak feedback regime ($C<<1$) the self-mixing signal shows a cosine function shape, which results in the ambiguity of the displacement direction. In weak feedback regime ($0.1<C<1$) the signal shape gets distorted and has a non-symmetrical shape. For stable interferometric displacement measurement that are non-ambiguous in direction, the feedback parameter is typically required to be at the moderate regime ($1<C<4.6$). Further increase of feedback parameter ($C>4.6$) results in entering the strong feedback regime, where multiple switchings per period may occur, and the measurement is affected by an error. Working in moderate feedback regime, at each displacement of half laser wavelength ($\lambda/2$) a fringe forms. The resultant signal shows a saw-tooth shape. By fringe-counting the total displacement (Δs) is calculated as:

$$\Delta s = n_{frg} \cdot \lambda/2 \tag{1}$$

where n_{frg} represents number of fringes. The saw-tooth signal shape of SMI also provides the displacement direction.

During the laser-material interaction with ns pulses, the pulse duration is long enough to generate thermal interaction that will generate vapour and molten phases of the material. In the initial phase of this interaction, plasma can also form from the material vapour. The pressure exerted on the molten phase by the vapour and plasma can cause material ejection [30]. One of the main concerns regarding the feasibility of the SMI for ablation measurements, is related to these physical changes modifying the optical properties in the space close to the hole, as the measurement beam should pass through turbid media [31]. As depicted in Fig. 1.b., the measurement beam encounters the ablation products namely, plasma, shockwave and plume which may scatter the beam and generate coherence loss. These factors can alter the optical feedback parameter and eventually the measurement signal can be lost. Moreover, the machined area differs from the initial surface in terms of both reflectivity and geometry. Speckle formation is also expected due to the changes in the surface morphology [32]. The use of side gas has been found to overcome the problems related to plume generation [23]. On the other hand, speckle effects are intrinsically difficult to tackle due to the fact that the measurement beam should pass through the realized hole as it is formed.

The SMI used in this work was realized using off-the-shelf components. The design criteria are explained in detail by Demir et. al. [23]. A GaAlAs laser diode with a multi-quantum well structure (HL7851G from Hitachi, Ibaraki, Japan) was used as the light source. Emission wavelength of the interferometer was 785 nm, resultantly the depth measurement resolution obtainable by simple fringe counting is half wavelength, at stable conditions is equal to 392.5 nm, which might drift ±2 nm due to temperature and current variations. The monitor photodiode current was converted by a single stage trans-impedance amplifier, realized by a transimpedance amplifier (OPA380 from Texas Instruments, Dallas, TX, USA) with gain equal to 420 kΩ. In these conditions, the bandwidth (BW) of the interferometer was about 1 MHz, allowing to capture the fast ablation phenomenon and obtain signals with good signal to noise ratio. The SMI signal was acquired with a digital oscilloscope characterized by 350 MHz maximum bandwidth, 5 GS/s sampling rate and $16 \cdot 10_6$ record length (TDS5034B from Tektronix, Oregon, USA).

The used processing laser was a master oscillator power amplifier (MOPA) fibre laser operating with green wavelength (YLPG-5 from IPG Photonics, Oxford, MA, USA). The measured average and estimated maximum peak powers are 6 W and 16 kW respectively. The processing laser is characterized by a delay and ramped emission in the initial phase of the emission [23]. In order to control the number of pulses emitted, the emission delay was measured for all experimented conditions and was added to effective drilling time for piloting the laser with the correct modulation duration. In the following graphs, the drilling time after the emission delay is exhibited. The processing beam was combined with the beam of the self-mixing interferometer with a dichroic mirror (DMLP567 from Thorlabs, Newton, NJ, USA). The beams

were focused using an achromatic lens with 100 mm focal length (AC254-100-A-ML from Thorlabs) and launched onto the workpiece on the same point (see Fig. 2). The main specifications of the processing and measurement lasers are summarized in Table I.

3. Performance of the self-mixing interferometer

The monitoring system was evaluated during the percussion microdrilling of TiAlN ceramic coating deposited on AISI D2 tool steel (Balinit Lumena from Oerlikon Balzers, Balzers, Liechtenstein). The coating thickness was measured as 12.1 ± 0.7 µm. Measured average surface roughness was 0.15 ± 0.02 µm. Laser percussion microdrilling was the used processing strategy, which is the basis of point-by-point laser surface texturing. In particular, for its application in laser ablation, the measurement error should not depend on the ablation depth, hence the laser ablation conditions. Moreover, the SMI system should be able to reveal ablation depth change with error margin lower than the variability of the coating thickness.

Therefore, the performance measurement of the SMI system was evaluated in laser microdrilling conditions generating hole depths below and beyond the coating thickness. The system is required to perform well independently of the processing conditions, hence, the whole feasibility range producing hole depths between 1 and 13 µm was explored. In this way, similar hole depths could be obtained using different laser process conditions. In order to evaluate the depth increase as a function of the laser parameters, 4 levels of pulse energy (E), 5 levels of number of pulses (N) and 2 levels of pulse repetition rate (PRR) were selected (see Table II). Experiments were applied using N_2 side gas jet at 1 bar to avoid signal loss due to ablation plume. All experimental conditions were repeated 5 times. Hole depth was measured offline, from the acquired SMI signals through manual fringe counting (h_{SMI}). The accuracy of the SMI measurements was determined in comparison to a conventional surface geometry measurement device (InfiniteFocus from Alicona, Graz, Austria) based on focus variation microscopy (FVM). Three-dimensional image of each hole was acquired using 50X magnification lens. In this configuration, vertical and horizontal resolutions were 12 nm and 1 µm respectively. The hole depth (h_{FVM}) was determined as the distance of the lowest point of the acquired hole with respect to the surface, as shown in Fig. 3. Fig. 3.c shows the self-mixing signal acquired during the ablation procedure: the fringes are clearly measurable and indicate a continuous growth of the hole during the drilling time.

Depth measurements were compared pairwise on each single hole, defining the measurement error (e) of SMI as:

$$e = h_{SMI} - h_{FVM} \tag{2}$$

The repeatability of the focus variation microscopy device used for measurement comparison was also analysed by designed experiments. Three conditions (K) representing low (average h_{FVM}=2.99 μm), medium (average h_{FVM}=6.39 μm) and high (average h_{FVM}=12.07 μm) hole depths were chosen. The chosen holes were acquired with the FVM 5 times. Each acquisition was also measured 5 times. All the acquisitions and measurements were carried out in random order. The resultant experimental plan was composed of Condition (K) with 3 levels, Acquisition repetition (AR) with 5 levels and Measurement repetition (MR) with 5 levels as the investigated factors. Analysis of variance (ANOVA) was applied on the measurement results. Bonferroni criteria was applied to test the statistical significance of the parameters and their interaction. Overall level of statistical significance, family error (α_{FAM}) was set at 5%. Accordingly, statistical significance level for each parameter and interaction was calculated as α_{FAM}/g, where g is the total number of statistical tests in ANOVA. For statistical significance, the p-value associated to a parameter or interaction has to be smaller than this calculated value [33]. Table III reports the results of analysis of variance. With three parameters and three second order interactions, the statistical significance for each test is 0.83%. It can be observed that the only significant parameter over the measured depth is Condition (K), hence the measured hole depth itself (p-value<0.83%). The acquisition and measurement repetitions and their interactions do not significantly alter the outcome of the measurement. In particular, the standard deviation pooled over different acquisition and measurement repetitions were 45 nm, 99 nm and 92 nm for low, medium and high hole-depths respectively. Such values are well below the resolution of the SMI employing fringe counting used in the experimentation, rendering FVM a suitable device for the performance evaluation of SMI.

4. Results

4.1.Self-mixing interferometry signal characteristics

Fig. 4 compares the SMI signals obtained during stable and disturbed conditions. The signal shown in Fig. 4.a. represents the conventional SMI signal in moderate feedback regime obtained during the displacement of a metallic target. The signal shows high amplitude (500 mV peak to peak fringe amplitude) and the saw-tooth shape is well-defined. One of the important issues related to measurement stability is the mode hopping phenomenon. In mode hopping the emission wavelength of the diode laser changes making discrete jumps, since the laser switches from one longitudinal mode to another [34]. Mode hopping is caused by laser case temperature, injection current and optical feedback. Both case temperature and injection current were kept stable during the experiments. However, the optical feedback was variable since the ablation phenomenon also changes the optical properties of the material surface during the process [35,36]. The material reflectivity and surface curvature are both varied throughout the process. Moreover,

within this measurement scheme the SMI is focused to a small spot increasing the intensity on a small area. Due to the low surface roughness of the material and at normal incidence, such as the one present in this work, the reflected light amount is expected to be higher and scattering is expected to be lower compared to rough and diffusive surfaces [37]. Hence, the amount of back reflected light may be excessive during the operation, causing the system to operate in the so-called strong feedback regime (C>4.6). In this regime, SMI measurements are not always possible. Due to all these factors, the system is also prone to mode hopping. Fig. 4.b demonstrates mode hopping phenomenon occurred during the placement of the workpiece. Mode hopping requires careful adjustment of the diaphragm in the optical chain to avoid entering in strong feedback regime, but also allowing enough optical feedback to work in moderate feedback regimes.

Another issue is related to the used process gas in the laser microdrilling process. As a matter of fact, an interferometer will measure the change in optical path difference, which can be induced by a change in distance, in refractive index or both [38]. Refractive index of air is 1.0002751 at 785 nm wavelength [39]. For the same wavelength refractive index of N_2 is reasonably close to air being 1.0002963, since this gas corresponds to the major component in air [40]. On the other hand the refractive index of He is 1.00003481, much smaller [41]. Hence, the He flow under the SMI generates fringes due to refractive index variation without any target displacement as shown in Fig. 4.c. Accordingly, the method is not suitable, if a process gas with refractive index very different from the ambient atmosphere is blown over the measurement area.

On the other hand, the SMI signals acquired during the laser microdrilling process are remarkably different from the signals obtained in conventional displacement measurement conditions. The signals shown in Fig. 4.d and 4.e represent SMI signals obtained during ablation process. It can be observed that the faster edge of the saw-tooth shape is less steep. The peak to peak fringe amplitude in this case is around 50 mV. The present fringe amplitude during laser ablation is about 5 times higher compared to the previous work by the authors' group, where higher BW (35 kHz) was employed [23]. The results demonstrate that 1 MHz BW level is more suitable as dynamic features of the signal are not compromised with higher signal to noise ratio. Therefore, the feedback parameter is decreased; however, the operation is still in moderate feedback regime. Due to the previously described changes in optical properties of the machined surface, the amount of reflected light can reduce, which also reduces the feedback parameter. Another common feature of the SMI signals in ablation monitoring is the ascending or descending slopes around the signal average value. This characteristic is attributed to the speckle phenomenon present in the so called non-cooperating targets [32]. In conventional SMI measurements signal average shifts from zero due to target surface scanning (see Fig. 4.e). The scattered light causes speckle formation. Consequently, signal fading and deformation, as

well as fringe amplitude variation occur. During the laser microdrilling operation the target changes the surface geometry, hence speckle formation is inevitable. The presence of these defects renders automated fringe counting difficult and in some cases impossible. Signal correction to overcome speckle effects is evidently vital for this purpose. Automated fringe counting and moreover signal analysis for retrieving the displacement within incomplete fringes should be considered, together with elaboration algorithm working in the frequency domain [42].

Another important feature of the SMI signals during the laser microdrilling process is related to the delay in the occurrence of the first fringe. This is expected to be due to the ramped emission profile in the initial part of the pulse train, which generates a reduced ablation rate. Hence, SMI is capable of measuring the changes in the ablation rate even within the displacement of a single fringe.

During ablation monitoring, these defects were present. A primary distinction was carried out for the readability of the signals as easy and difficult. The SMI signal shown in Fig. 4.d depicts an easy read-out as signal deformation due to reduced feedback parameter and speckle are limited. On the other hand the SMI signal in Fig. 4.e is an example for difficult read-out due to a marked speckle effect and variable signal shape due to changing feedback parameter. The occurrence of difficult read-out signals was high, consisting of 55% of the 199 acquired signals. In the analysis, all signals were used for fringe counting, however, the effect of signal quality on the error was also evaluated.

4.2. Evaluation of measurement error

Fig. 5 reports the hole depth measurements obtained by FVM, over the experimented region as a function of process parameters. It can be observed that within the experimented region, hole depths could vary between 1.5 μm and 13 μm. Both pulse energy and number of pulses were effective in increasing hole depth, whereas the influence of pulse repetition rate was limited. Fig. 6 compares the hole geometries obtained with different process parameter combinations. The holes exhibit slight ellipticity, which can be only partially attributed to the processing laser beam shape. The geometrical imperfections components of the used experimental optical system and their alignment is also expected to contribute. It can also be observed that the bottom of the blind holes show significantly different roughness profile compared to the non-machined surface. Such roughness profile change can cause change in the reflectivity of the material at the bottom of the hole, hence reduce the optical feedback. Moreover, roughness profile induces a variable surface profile at the bottom of the hole, which can alter the measured displacement. However, this second

contribution is expected to be much less significant being in a smaller dimensional range compared to the resolution obtained by fringe counting. The impact of roughness can be more relevant with improved resolution of the device through signal processing. The images show that holes with similar depth could be achieved with different diameters and vice versa. In particular, the holes shown in Fig. 6.a and Fig. 6.b are characterized by similar low depth (average h_{FVM}=3.38 μm), whereas the ones in Fig. 6.c and Fig. 6.d exhibit high depth (average h_{FVM}=10.38 μm). On the other hand, the holes Fig. 6.a and Fig. 6.c show similar small diameter (average D=18 μm), whereas Fig. 6.b and Fig. 6.d show holes with similar and larger diameters (average D=24 μm). Accordingly, within the experimental campaign the effect of the hole diameter is included.

Fig. 7.a-d exhibits SMI signals of obtained in increasing number of pulses with fixed pulse energy and pulse repetition rate levels. The Fig. clearly depicts that the number of fringes increases with the number of pulses, following the same trend observed with the FVM measurements. Fig. 7.e shows the hole depth measured by SMI employing simple fringe counting. It can be observed that the results are very close to the measurements obtained by FVM and maintain the same linear increase as function of number of pulses (N) and pulse energy (E), whereas no significant effect of pulse repetition rate (PRR) is visible.

Over the total number of 200 experiments resulting from 40 experimental conditions and 5 replications for each, only one was not included in the further qualitative and statistical analyses due to experimental error. Each microhole realized experimented condition was measured with FVM and the acquired SMI was used to measure the depth of the same hole. In Fig. 8.a. the error of SMI measurements is shown as a function of the process parameters and signal quality classification. The error classes are also highlighted as missing or excess fringe counts with the dashed lines. Fig. 8.b. shows these error classes in their corresponding occurrence percentage. The main results coming from the analysis can be listed as below.

1. SMI signal quality is adequate to avoid misreading in general. The SMI measurements are clustered around same values within the same processing conditions. This is due to the discrete incremental steps in the measurement based on fringe counting and the fact that all the measurements are multiples of $\lambda/2$. As shown in Fig. 8.a., the overall results show that the error is confined between 0 and $-\lambda$=-0.785 μm. As a matter of fact, all error values falling below this range (between $-\lambda$ and -2λ) correspond to signals with difficult read-out.

2. The measurement error is independent from the processing conditions. As depicted in Fig. 8.a, the measurement error does not follow a certain trend across the experimental range. The dependency of error on the processing conditions was evaluated with analysis of variance (ANOVA). Bonferroni criteria was

applied with α_{FAM}=5%. With three parameters, three second order interactions, and one third order interaction, the statistical significance for each test is 0.71%. As depicted in Table IV, none of the parameters was found to be significant. This result depicts that the SMI measurement is not affected by the hole geometry, particularly by diameter or depth. The measurement campaign shows that the same depth can be obtained in different time durations, using lower or higher pulse repetition rates. Therefore, it can be concluded that the error does not depend on the depth increase rate as well.

3. Measurement error margin is lower than the variability of the coating thickness. The majority of the measurement error (76% of the whole experimented range) falls between 0 and 1 missing fringe range (between 0 and -λ/2). This range represents the capability of the device, since the error is lower than the resolution obtained by fringe counting (λ/2=0.393 nm). Hence, in the majority of the cases the SMI error is acceptable for the application. Only in 6% of the experimented range (11 measurements) the error corresponds to more than 1 missing fringe (between –λ and -2λ), which is larger than the thickness variation. The device is capable of measuring with adequate error margin in the most critical region, the coating/substrate interface.

4. SMI measurements underestimate the hole depth. In Fig. 8.a, it can be observed that the error is accumulated around negative values, which depicts that the SMI system tends to underestimate the hole depth. This phenomenon is due to the functioning principle of SMI. A fringe will form when the displacement is increased by λ/2. When, the displacement ends without reaching a multiple of λ/2, the remaining part will generate an incomplete fringe. Such increment is not captured in fringe counting but can be estimated by signal processing. As shown in Fig. 9, during the microdrilling process the hole depths that fall between two discrete fringe numbers will be measured with a smaller depth compared to the real one. Due to this reason, only the region between –λ/2 and 0 can be considered as correct measurements within the capability of the device. Regarding other error classes, the positive error obtained in region between 0 and λ/2 is due to signal errors. The range between –λ/2 and -λ corresponds to one missing fringe and is acceptable for measurements based on manual fringe counting. Finally, in the region between –λ and –2λ error classes of 2 and 3 missing fringes exist. In these error classes, the signal quality was always found to be low, which is the main cause for the error.

5. Conclusions

In this work the use of SMI for ablation depth monitoring of TiAlN ceramic coating was demonstrated. For the first time, the measurement accuracy of SMI for ablation depth monitoring was methodologically investigated in a large processing range. In particular, the performance of the measurement method was

evaluated regarding the process requirements. For this purpose, the signal characteristics of SMI measurement system were investigated. It was observed that the SMI measurements was sensitive to increased optical feedback due to tightly focused beam and refractive index changes that may occur due to the used side gas jet. Moreover, the SMI signals suffered from changes in reflectivity and speckle formation during ablation, which significantly reduce the signal quality in comparison to signals obtained in conventional applications. The measurement error of SMI was found to be below resolution obtainable by simple fringe counting ($\lambda/2$=0.393 μm) for the larger part of the experimental range (76%). Overall, the error did not exceed 2λ=1.57 μm. The SMI measurements were also found to underestimate the hole depth due to incomplete fringe formation.

Under the light of the obtained results, it can be concluded that the SMI measurement system is capable of measuring the ablation depth, with an error margin below the coating thickness variation. Moreover, the results show that further reduction of measurement error is possible through improving the signal quality. Improvement of the signal quality during the measurement is limited due to the complicated nature of the ablation process, through which the drilled microhole acts as a non-cooperating target. A more feasible way for improved measurement performance appears to be in the post-processing stage. The complexity of the post-processing strategies, however, would increase the computation time and render eventually the online use of this monitoring method more difficult. Accordingly, the acceptable error margin should be considered for the given application. Increasing the device resolution by reducing the wavelength is another possibility for reducing error margin. It should be noted that the chosen wavelength should not coincide with the plasma luminescence of the workpiece material to avoid its integration to the PD, and the electronic bandwidth should be matched to acquire the higher number of fringes observed in the same drilling time.

Acknowledgements

The authors gratefully acknowledge Prof. Quirico Semeraro for the valuable discussion and support in data analysis phase. IPG Italy is acknowledged for providing the green fiber laser source.

References

1. A.G. Demir, N. Lecis, B. Previtali, and D. Ugues, "Scratch resistance of fibre laser surface textured TiN coatings," *Surf. Eng.,* vol. 29, no. 9, pp. 654-659, Oct. 2013
2. A.G. Demir, K. Pangovski, W. O'Neill, and B. Previtali, "Laser micromachining of TiN coatings with variable pulse durations and shapes in ns regime," *Surf. Coat. Technol.,* vol. 258, pp. 240-248, Nov. 2015.
3. L. Vandoni, A.G. Demir, B. Previtali, N. Lecis, and D. Ugues, "Wear behavior of fiber laser textured TiN coatings in a heavy loaded sliding regime," *Materials,* vol. 5, no. 11, pp. 2360-2382, Nov. 2012.
4. T. Kurita, T. Ono, and T. Nakai, "A study of processed area monitoring using the strength of YAG laser processing sound," *J. Mater. Process. Technol.* vol. 112, pp. 37–42, May 2001.
5. M. Stafe, C. Negutu, and I.M. Popescu, "Real-time determination and control of the laser-drilled holes depth," *Shock Waves,* vol. 14, no. 1–2, pp. 123–126, Jun. 2005
6. D.P. Hand, C. Peters, F.M. Haran, and J.D.C. Jones. "A fibre-optic based sensor for optimization and evaluation of the laser percussion drilling process," *Meas. Sci. Technol.,* vol. 8, pp. 587–592, Jun. 1997
7. A. Stournaras, K. Salonitis, and G. Chryssolouris, "Optical emissions for monitoring of the percussion laser drilling process," *Int. J. Adv. Manuf. Technol.*, vol. 46, no. 5–8, pp. 589–603, Jan. 2010
8. V. Kanicky, J. Musil, and J.-M. Mermet, "Determination of Zr and Ti in 3-μm-thick ZrTiN ceramic coating using laser ablation inductively coupled plasma atomic emission spectrometry," *Appl. Spectrosc.*, vol. 51, no. 7, 1037–1041, Jul. 1997
9. F. Le Guern, F. Brygo, P. Fichet, E. Gauthier, C. Hubert, C. Lascoutuna, D. Menut, S. Mousset, A. Semerok, M. Tabarant, and J.M. Weulersse, "Co-deposited layer characterisation and removal control by optical emission spectroscopy coupled to nano-second laser ablation," *Fusion Eng. Des.*, vol. 81, pp. 1503–1509, Feb. 2006
10. H. Balzer, M. Hoehne, V. Sturm, and R. Noll, "Online coating thickness measurement and depth profiling of zinc coated sheet steel by laser induced breakdown spectroscopy," *Spectrochim. Acta Part B*, vol. 60, pp. 1172–1178, Aug. 2005
11. C. Grisolia, A. Semerok, J. Weulersse, F. Leguern, S. Fomichev, F. Brygo, P. Fichet, P. Thro, P. Coad, and N. Bekris, "In-situ tokamak laser applications for detritiation and co-deposited layers studied," *J. Nucl. Mater.,* vol. 363–365, pp. 1138–1147, Jun. 2007

12. J. Ruiz, A. Gonzalez, L.M. Cabalin, and J.J. Laserna, “On-line laser induced breakdown spectroscopy determination of magnesium coating thickness on electrolytically galvanized steel in motion,” *Appl. Spectrosc.*, vol. 64, no. 12, pp. 1342–1349, Dec. 2010
13. S. Döring, S. Richter, S. Nolte, and A. Tünnermann, “In situ imaging of hole shape evolution in ultrashort pulse laser drilling,” *Opt. Express*, vol. 18, no. 19, pp. 20395–400, Sep. 2010.
14. D.G. Papazoglou, V. Papadakis, and D. Anglos, “In situ interferometric depth and topography monitoring in LIBS elemental profiling of multilayer structures,” *J. Anal. At. Spectrom.*, vol. 19, pp. 483-488, 2004.
15. P.J.L. Webster, J.X.Z. Yu, B.Y.C. Leung, M.D. Anderson, V.X.D. Yang, and M. James, “In situ 24 kHz coherent imaging of morphology change in laser percussion drilling,” *Opt. Express*, vol. 35, no. 5, pp. 646–648, Mar. 2010
16. P.J.L. Webster, L.G. Wright, K.D. Mortimer, B.Y. Leung, J.X.Z. Yu, and JM Fraser, “Automatic real-time guidance of laser machining with inline coherent imaging,” *J. Laser Appl.*, vol. 23 no. 2, p. 022001, May. 2011.
17. B.Y.C. Leung, P.J.L. Webster, J.M. Fraser, and V.X.D. Yang, “Realtime guidance of thermal and ultrashort pulsed laser ablation in hard tissue using inline coherent imaging,” *Lasers Surg. Med.*, vol. 44, 249–256, Mar. 2012
18. Y. Ji, A.W. Grindal, P.J.L. Webster, and J.M. Fraser, “Real-time depth monitoring and control of laser machining through scanning beam delivery system,” *J. Phys. D: Appl. Phys.*, vol 48, p. 155301, Mar. 2015
19. S. Donati, “Developing self-mixing interferometry for instrumentation and measurements,” *Laser Photon. Rev.* vol. 6, pp. 393-417, May 2012
20. F. P. Mezzapesa, A. Ancona, T. Sibillano, F. De Lucia, M. Dabbicco, P. M. Lugarà, and G. Scamarcio, “High-resolution monitoring of the hole depth during ultrafast laser ablation drilling by diode laser self-mixing interferometry,” *Opt. Lett.*, vol. 36, no. 6, pp. 822–824, Mar. 2011.
21. F. P. Mezzapesa, V. Spagnolo, A. Ancona, and G. Scamarcio, “Detection of ultrafast laser ablation using quantum cascade laser-based sensing,” *Appl. Phys. Lett.*, vol. 101, no. 17, p. 171107, Oct. 2012
22. F. P. Mezzapesa, T. Sibillano, F. Di Niso, A. Ancona, P. M. Lugarà, M. Dabbicco, and G. Scamarcio, “Real time ablation rate measurement during high aspect-ratio hole drilling with a 120-ps fiber laser,” *Opt. Express*, vol. 20, no. 1, pp. 663-671, Jan. 2012

23. A. G. Demir, B. Previtali, A. Magnani, A. Pesatori, and M. Norgia, “Application of self-mixing interferometry for depth monitoring in the ablation of TiN coatings,” *J. Laser Appl.*, vol. 27, no. S2, p. S28005, Feb. 2015.
24. U. Zabit, F. Bony, T. Bosch, and A. D. Rakic, “A Self-Mixing Displacement Sensor With Fringe-Loss Compensation for Harmonic Vibrations,” *IEEE Photonics Technol. Lett.*, vol. 22, no. 6, pp. 410–412, Mar. 2010
25. A. Magnani, A. Pesatori, and N. Norgia, “Real-Time Self-Mixing Interferometer for Long Distances,” *IEEE Trans. Instrum. Meas.*, vol. 63, no. 7, pp. 1804-1809, Jul. 2014.
26. M. Norgia, G. Giuliani, and S. Donati, “Absolute Distance Measurement with Improved Accuracy using Laser Diode Self–Mixing Interferometry in a Closed Loop,” *IEEE Trans. Instrum. Meas.* vol. 56 no. 5, pp. 1894 -1900, Oct. 2007.
27. A. Magnani, A. Pesatori, and M. Norgia, “Self-mixing vibrometer with real-time digital signal elaboration.,” *Appl. Opt.*, vol. 51, no. 21, pp. 5318–25, Jul. 2012.
28. M. Norgia, A. Pesatori, and L. Rovati, “Low-Cost Optical Flowmeter With Analog Front-End Electronics for Blood Extracorporeal Circulators,” *IEEE Trans. Instrum. Meas.* vol. 59, no. 5, pp. 1233-1239, May 2010
29. S.K. Ozdemir, I. Ohno, and S. Shinohara, “A comparative study for the assessment on blood flow measurement using self-mixing laser speckle interferometer,” *IEEE Trans. Instrum. Meas.*, vol. 57, no. 2, pp. 355-363, Feb. 2008.
30. B. N. Chichkov, C. Momma, S. Nolte, F. von Alvensleben, and A. Tünnermann, “Femtosecond, picosecond and nanosecond laser ablation of solids,” *Appl. Phys. A Mater. Sci. Process.*, vol. 63, no. 2, pp. 109–115, Jul. 1996.
31. C. Dunsby and P. M. W. French, “Techniques for depth-resolved imaging through turbid media including coherence-gated imaging,” *J. Phys. D. Appl. Phys.*, vol. 36, no. 14, pp. R207–R227, Jul. 2003
32. U. Zabit, O. D. Bernal, and T. Bosch, “Self-Mixing Laser Sensor for Large Displacements: Signal Recovery in the Presence of Speckle,” *IEEE Sens. J.*, vol. 13, no. 2, pp. 824–831, Feb. 2013.
33. D.C. Montgomery, *Design and Analysis of Experiments, 5th Ed*. New York, NY: John Wiley and Sons, 2001
34. P.J. Herre and U. Barabas, “Mode switching of Fabry-Perot laser diodes,” *IEEE J. Quant. Electron.*, vol. 25, no. 8, pp. 1794-99, 1989.

35. W. Schulz, U. Eppelt, and R. Poprawe, “Review on laser drilling I. Fundamentals, modeling, and simulation,” *J. Laser Appl.*, vol. 25, no. 1, p. 012006, Feb. 2013.
36. K. Pangovski, M. Sparkes, A. Cockburn, W. O. Neill, P. S. Teh, D. Lin, and D. Richardson, “Control of Material Transport Through Pulse Shape Manipulation — A Development Toward Designer Pulses,” *IEEE J. Sel. Top. Quantum Electron.*, vol. 20, no. 5, Sep. 2014.
37. D. Bergström, J. Powell, and A. F. H. Kaplan, “A ray-tracing analysis of the absorption of light by smooth and rough metal surfaces,” *J. Appl. Phys.*, vol. 101, no. 11, p. 113504, Jun. 2007.
38. P. Hariharan, *Basics of Interferometry, 2nd Ed.* Academic Press, 2006.
39. P.E. Ciddor, “Refractive index of air: new equations for the visible and near infrared,” *Appl. Optics*, vol. 35, pp. 1566-1573, 1996
40. E.R. Peck and B.N. Khanna, “Dispersion of nitrogen,” *J. Opt. Soc. Am.*, vol. 56, pp. 1059-63, 1963.
41. C.R. Mansfield and E.R. Peck, Dispersion of helium,” *J. Opt. Soc. Am.*, vol. 59, pp. 199-203, 1969.
42. M. Norgia and C. Svelto, “Novel Measurement Method for Signal Recovery in Optical Vibrometer,” *IEEE Trans. Instrum. Meas.*, vol. 57, no. 8, pp. 1703-1707, 2008.

List of figures

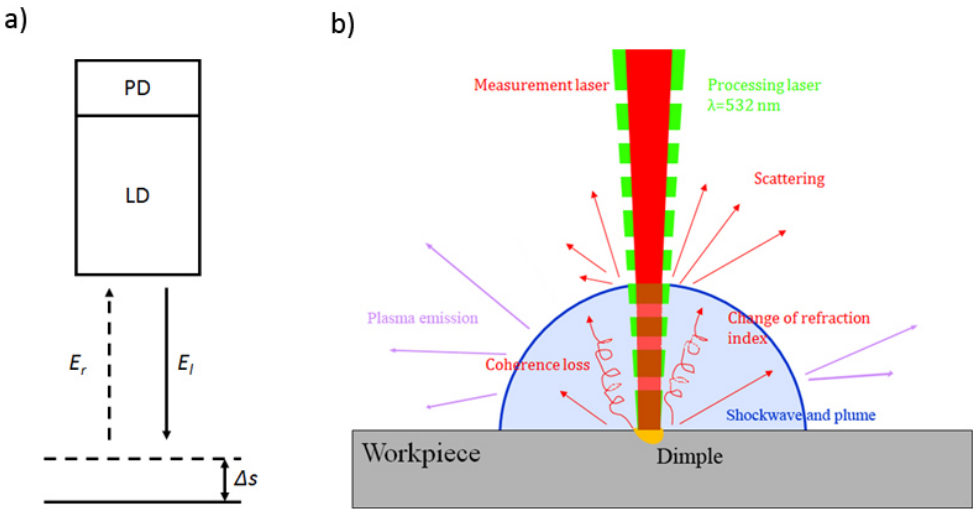

Fig. 1. a) The working principle of self-mixing interferometry for displacement measurement. b) Schematic representation of the optical changes around the surface vicinity due to ablation products, which are likely to disturb SMI measurements.

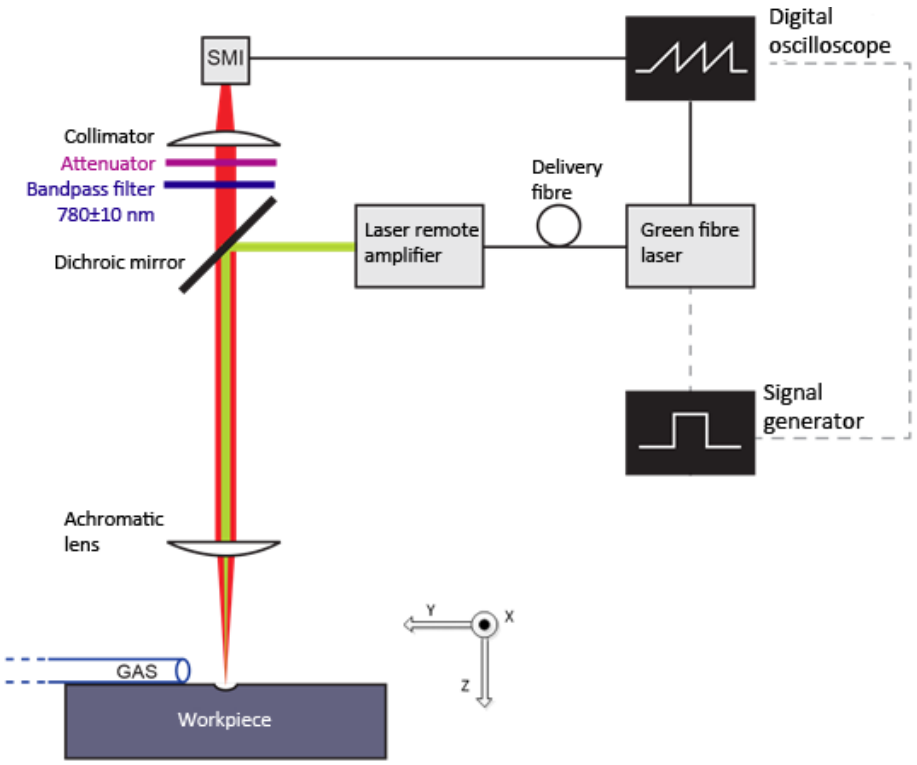

Fig. 2. Ablation monitoring setup consisting of the processing laser and self-mixing interferometer.

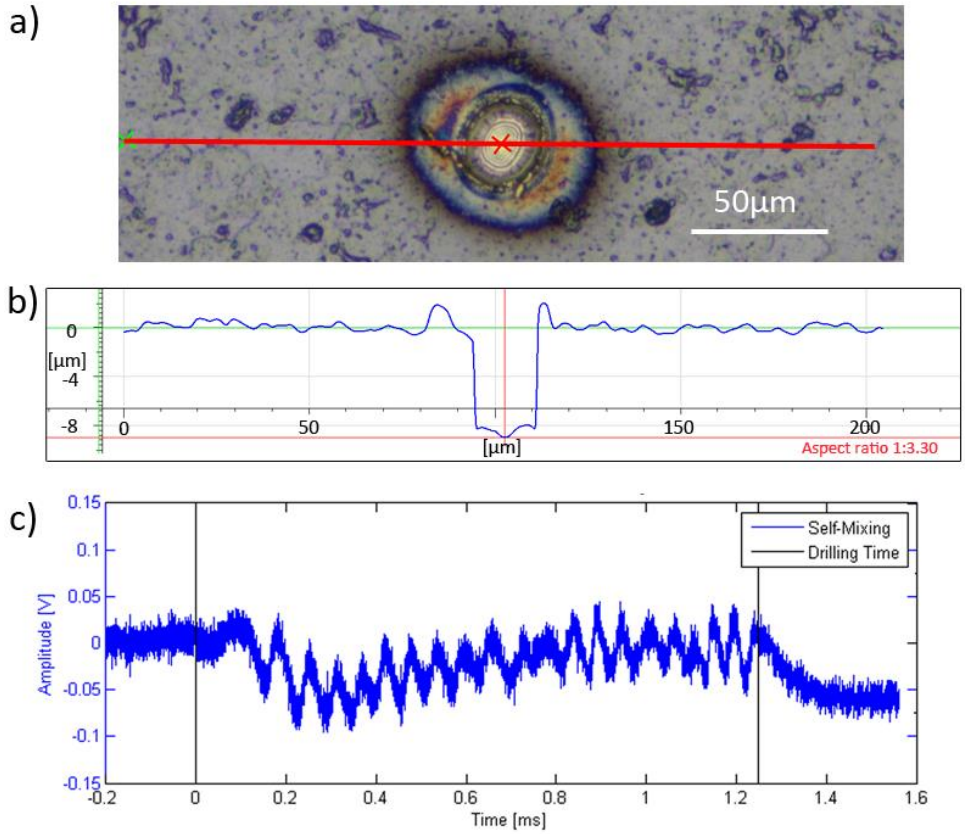

Fig. 3. Determination of hole depth with FVM and SMI (*E*=10 µJ, *PRR*=160 kHz, *N*=200). a) Real colour image acquired by FVM depicting the position of the depth profile, b) the corresponding depth profile; c) the SMI signal belonging to the hole.

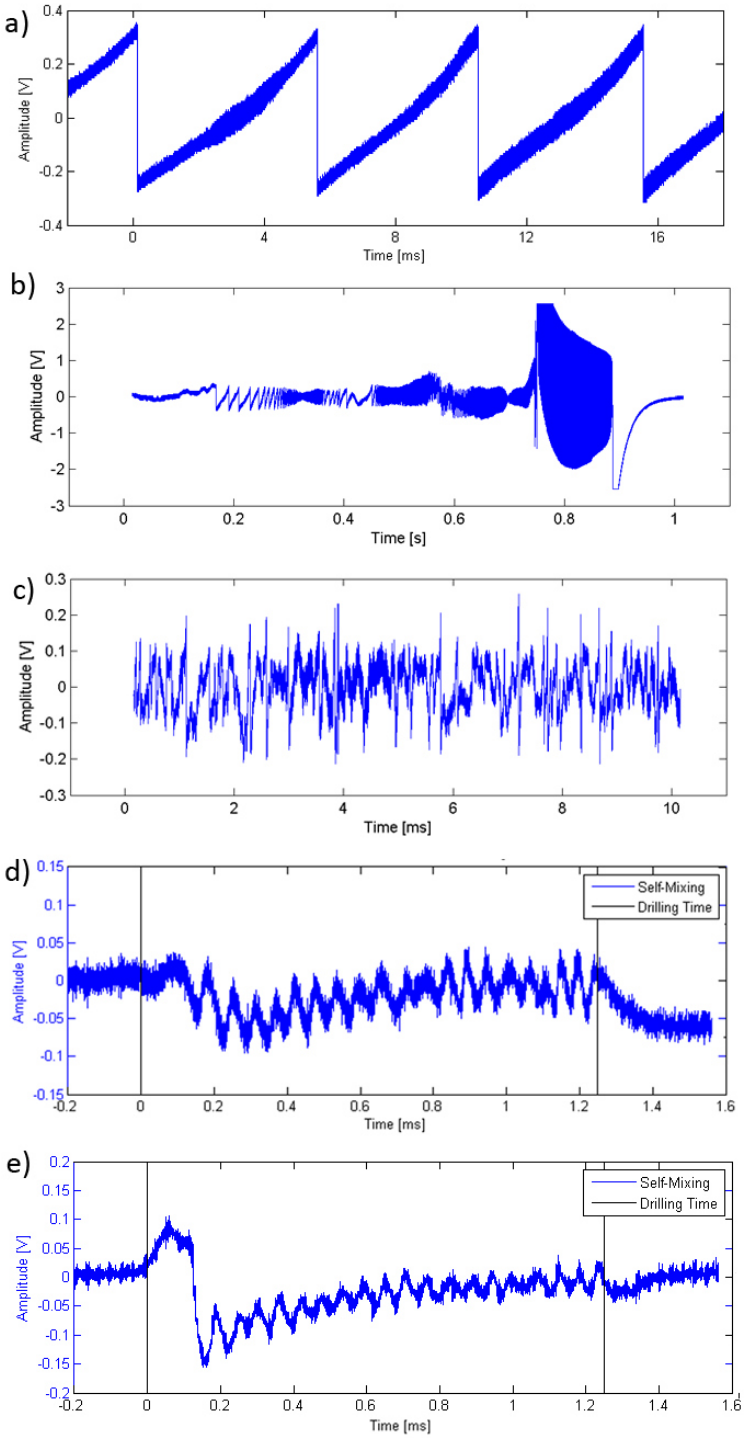

Fig. 4. SMI signals representing stable and disturbed measurement conditions. a) During the displacement of a metallic target, b) mode hopping caused by excessive back reflection from the remote target, c) without target displacement in presence of He flow, d) easy read-out signal type during microdrilling of TiAlN coating (E=10 µJ, PRR=160 kHz, N=200), e) difficult read-out signal type (E=10 µJ, PRR=160 kHz, N=200).

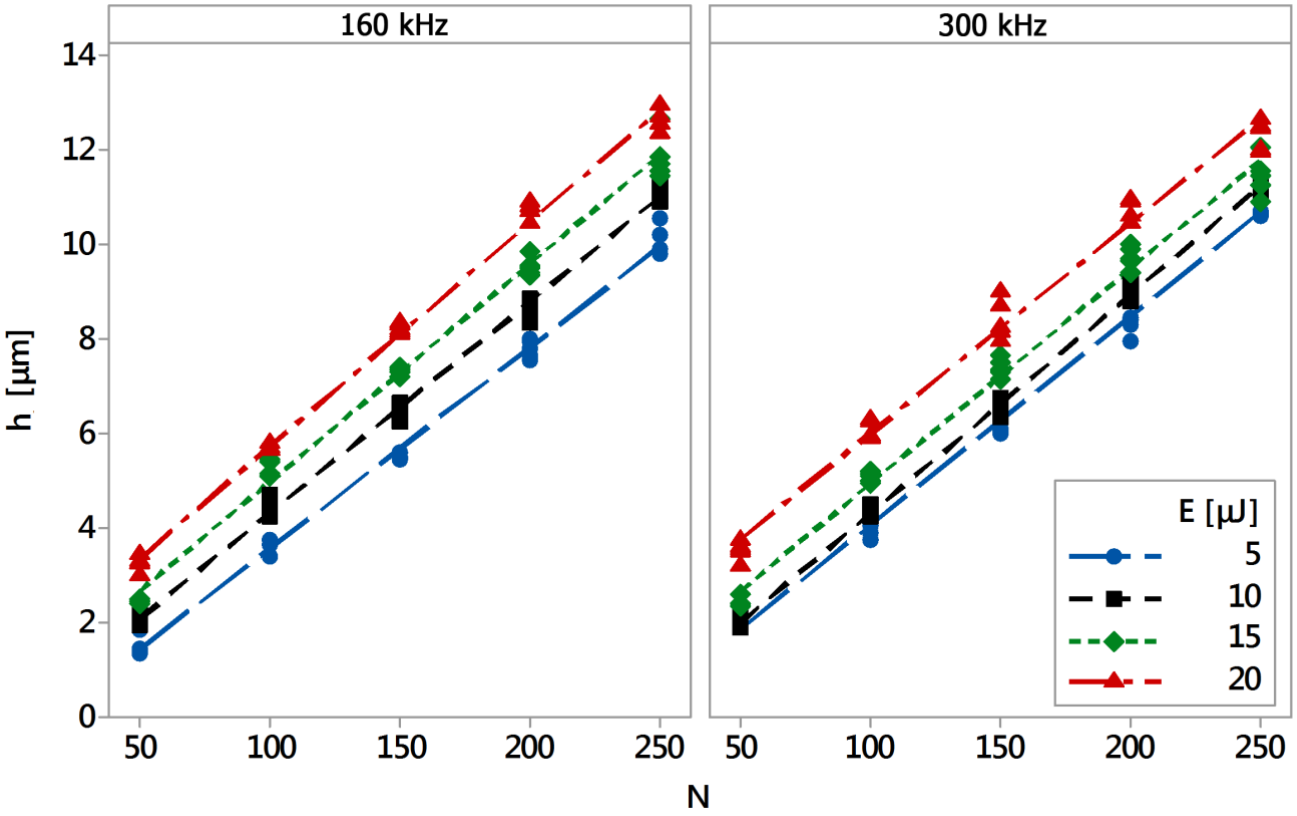

Fig. 5. Hole depth (*h*) as a function of process parameters pulse energy (*E*), number of pulses (*N*) and pulse repetition rate (*PRR*) measured by FVM.

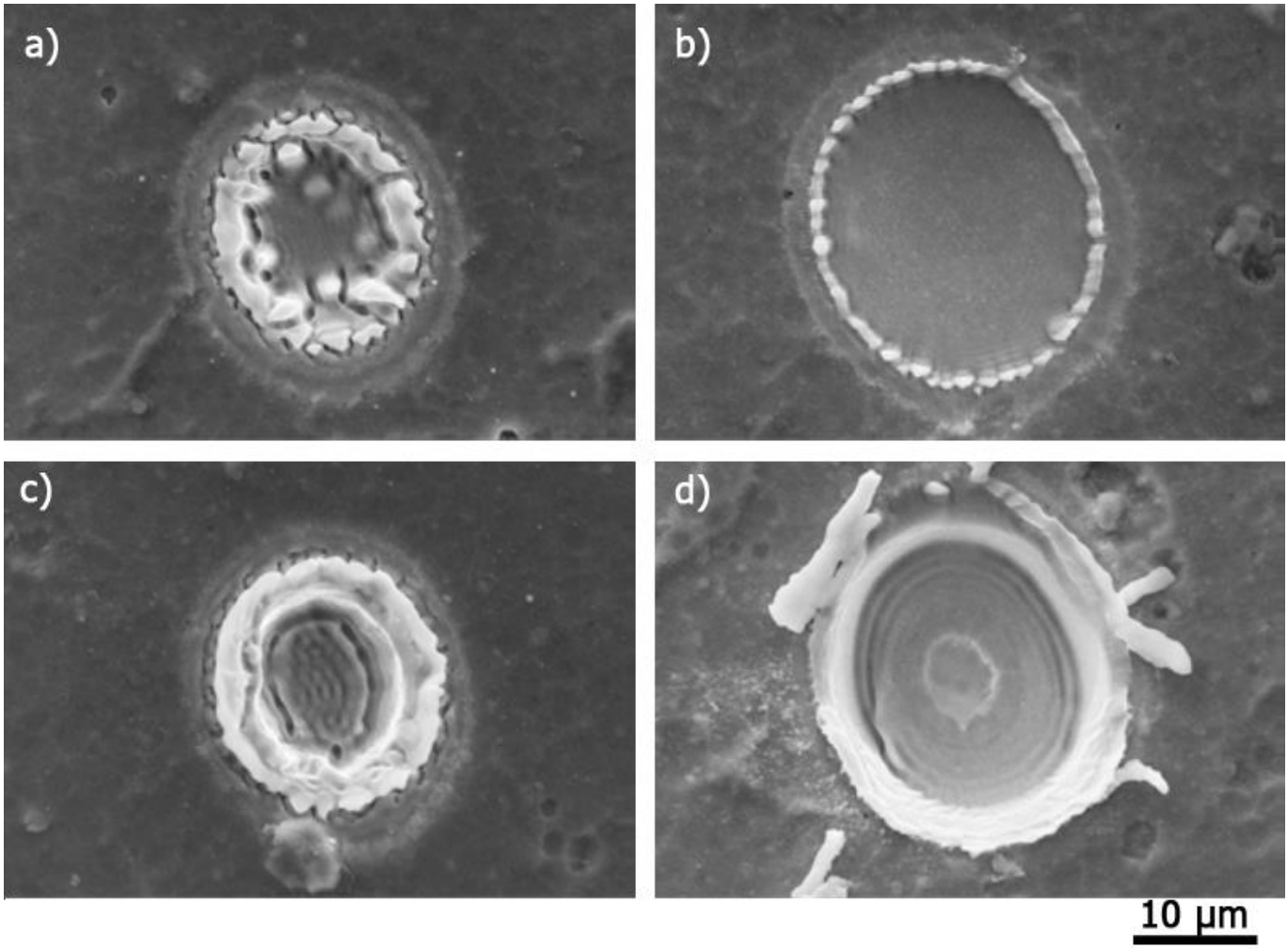

Fig. 6. Comparison of hole morphology obtained with different laser microdrilling parameters, showing similar depth and diameter conditions. a) *E*=5 µJ, *PRR*=160 kHz, *N*=100; b) *E*= 20 µJ, PRR=300 kHz, *N*=50; c) *E*=5 µJ, *PRR*=160 kHz, *N*=250; d) *E*=20 µJ, PRR=300 kHz, *N*=200;

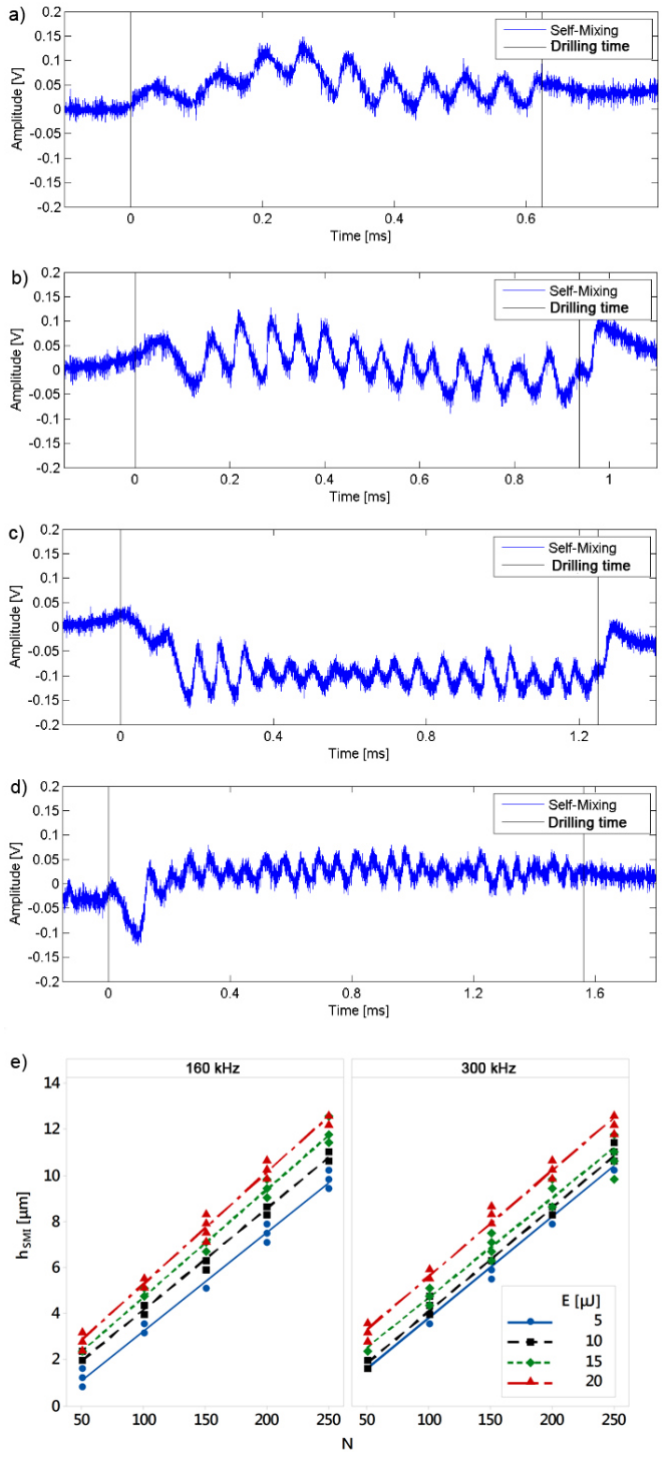

Fig. 7. SMI signal examples during the ablation of holes with different depths. Laser microdrilling parameters were E=10 µJ, PRR=160 kHz with variable number of pulses N. a) N=100, n_{frg}=10, h_{SMI}=3.93 µm; b) N=150, n_{frg}=16, h_{SMI}=6.28 µm; c) N=200, n_{frg}=22, h_{SMI}=8.64 µm; d) N=250, n_{frg}=28, h_{SMI}=10.21 µm; e) hole depth (h) as a function of process parameters pulse energy (E), number of pulses (N) and pulse repetition rate (PRR) measured by SMI.

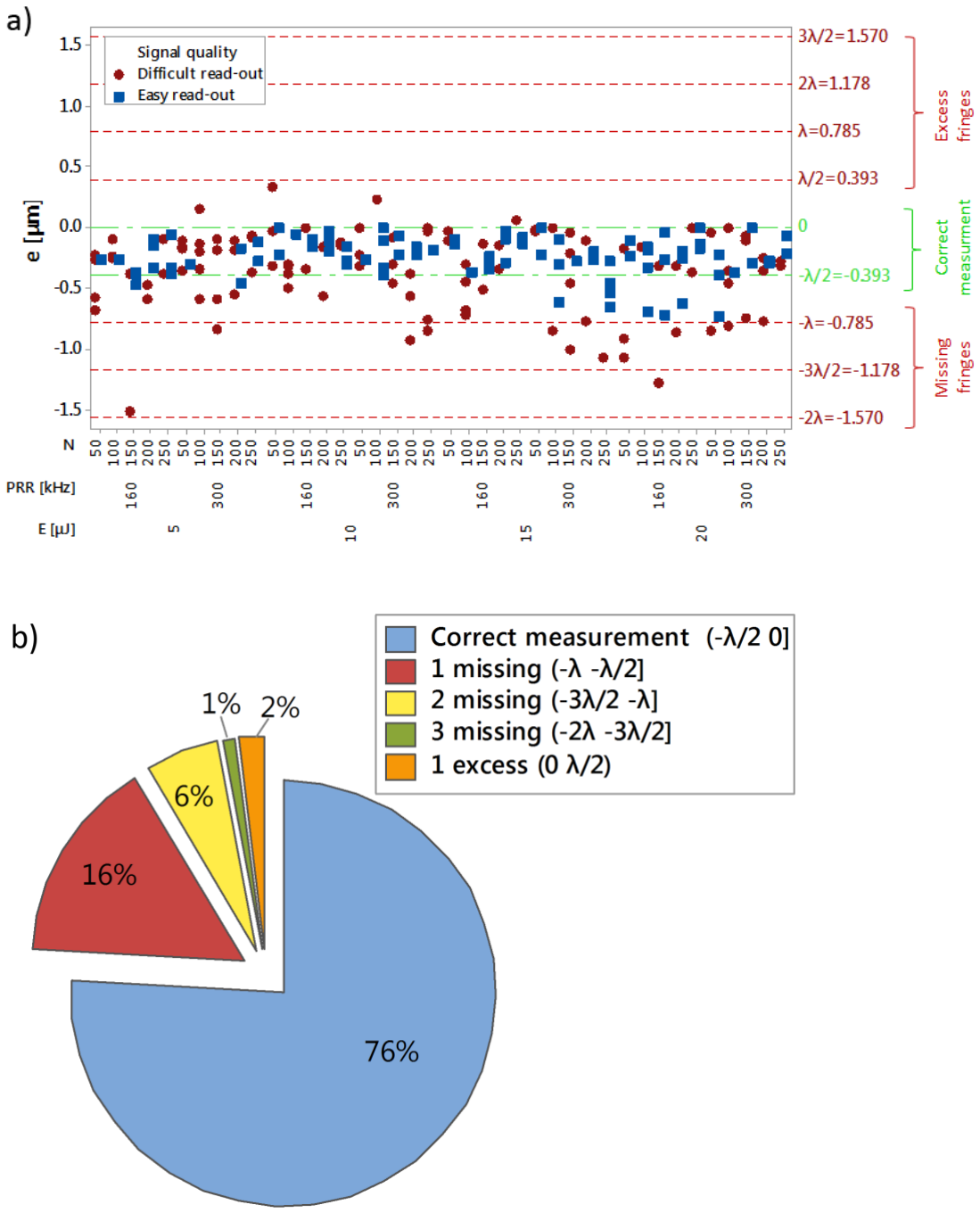

Fig. 8. a) Measurement error as a function of process parameters and signal quality. The dashed lines indicate the error classes as a function of fringe count. b) Occurrence percentage of the error classes. The percentages refer to 199 total number of measurements.

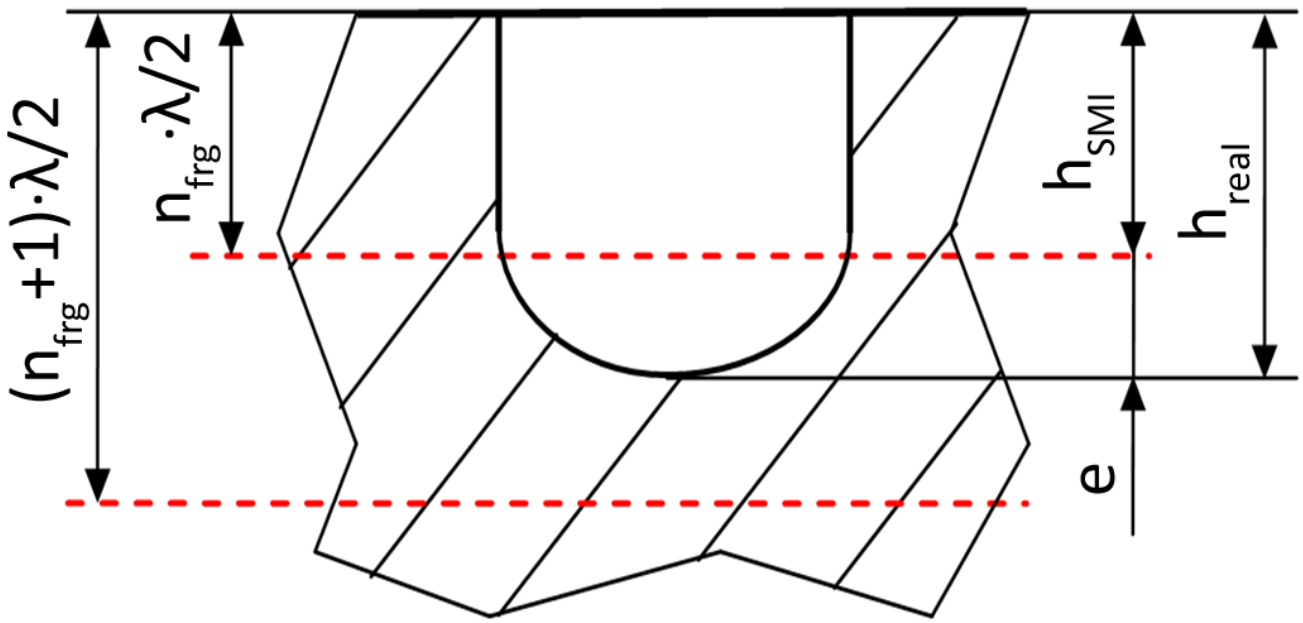

Fig. 9. Schematic representation of the underestimation error due to incomplete fringes.

List of tables

Table I. Main characteristics of the processing and measurement lasers.

Parameter	Processing	Measurement
Emission wavelength, λ	532 nm	785 nm
Emission type	Pulsed wave	Continuous wave
Output power, P	6 W (Average)	0.015 W
Pulse duration, τ	1.2 ns	n/a
Pulse repetition rate, PRR	20-300 kHz	n/a
Maximum pulse energy, E_{max}	20 µJ	n/a
Beam quality factor, M^2	1.1	1.2
Collimated beam diameter	3.49 mm	2.9 mm (fast axis) 5.1 mm (slow axis)
Focused beam diameter (f=100 mm), d_0	21.7 µm	41.4 µm (fast axis) 23.5 µm (slow axis)

Table II. Experimental plan for accuracy evaluation of the measurement system.

Fixed parameters		
Focal position	h_f [mm]	0
Varied parameters		
Pulse energy	E [µJ]	5, 10, 15, 20
Number of pulses	N [-]	50, 100, 150, 200, 250
Pulse repetition rate	PRR [kHz]	160, 300
Measured variable		
Hole depth measured with SMI	h_{SMI} [µm]	
Hole depth measured with FVM	h_{FVM} [µm]	

Table III. ANOVA table for hole depth measured by focus variation microscope h_{FVM} [µm]. *DF*: degrees of freedom; *F-value*: the test statistic used to determine whether the term is associated with the response; *P-value*: a probability that measures the evidence against statistical significance; *S*: standard deviation of how far the data values fall from the fitted values; R^2: percentage of variation in the response that is explained by the model; R^2_{adj}: the value of R^2 adjusted for the number of predictors in the model relative to the number of observations.

Source	DF	F-Value	P-Value
Condition (K)	2	86630.89	0
Acquisition repetition (AR)	4	1.06	0.391
Measurement repetition (MR)	4	2.09	0.105
K*AR	8	1.93	0.089
K*MR	8	0.45	0.880
AR*MR	16	1.00	0.48
Error	32		
Total	74		
S=0.078	R^2=99.98%	R^2_{adj}=99.96%	

Table IV. ANOVA table for measurement error *e* [µm]. *DF*: degrees of freedom; *F-value*: the test statistic used to determine whether the term is associated with the response; *P-value*: a probability that measures the evidence against statistical significance; *S*: standard deviation of how far the data values fall from the fitted values; R^2: percentage of variation in the response that is explained by the model; R^2_{adj}: the value of R^2 adjusted for the number of predictors in the model relative to the number of observations.

Source	DF	F-Value	P-Value
E [µJ]	3	1.74	0.161
PRR [kHz]	1	1.08	0.301
N	4	0.9	0.456
E [µJ]*PRR [kHz]	3	1.48	0.221
E [µJ]*N	12	2.26	0.011
PRR [kHz]*N	4	1.53	0.201
E [µJ]*PRR [kHz]*N	12	1.08	0.38
Error	157		
Total	196		
S=0.236	R^2=28.07%	R^2_{adj}=10.20%	